PCCP

ROYAL SOCIETY OF CHEMISTRY

PAPER

View Article Online
View Journal | View Issue

Cite this: *Phys. Chem. Chem. Phys.*, 2021, **23**, 347

Non-stoichiometric molybdenum sulfide clusters and their reactions with the hydrogen molecule†

Yan Chen,[ab] Jia-Jun Deng,*[ab] Wen-Wen Yao,[ab] Joseph Israel Gurti,[ab] Wei Li,[ab] Wen-Jie Wang,[ab] Jian-Xi Yao[cd] and Xun-Lei Ding*[ab]

Received 23rd August 2020,
Accepted 7th December 2020

DOI: 10.1039/d0cp04457a

rsc.li/pccp

Structures of non-stoichiometric Mo_xS_y clusters (x = 2–4; y = 2–10) were studied by density functional calculations with global optimization. Besides 1T phase like structures, a novel regular grid structure in which Mo atoms are well separated by S atoms was found, which might be used as a building-block to construct a new type of two-dimensional molybdenum sulfide monolayer. The hydrogen molecule prefers to be adsorbed onto Mo atoms rather than S atoms, and Mo atoms with less S coordination have a higher ability to adsorb H_2. In addition, the reaction pathways for H_2 dissociation were studied on two clusters with the highest H_2 adsorption energy (Mo_2S_4 and Mo_3S_3). The vacant bridge site of Mo–Mo in S-deficient clusters, which corresponds to the sulfur vacancy in the bulk phase MoS_2, is favored by H atom adsorption and plays an important role in the H atom transfer on Mo_xS_y clusters. Our results provide a new aspect to understand the reason why S defect in MoS_2 and MoS_2 with an Mo-edge could enhance the catalytic performance in the hydrogen evolution reaction.

Introduction

Hydrogen is being pursued as a future source of energy in the current transition process of fossil energy to clean energy.[1–3] As a vital approach to producing sustainable hydrogen, the hydrogen evolution reaction (HER, *e.g.*, water decomposition) has attracted more and more attention.[4] Advanced catalysts for the electrochemical HER are able to reduce the over-potential and thus improve the efficiency of this important electrochemical process. The most effective catalysts are platinum group metals, which are too expensive for a wide range of applications. It is an inevitable trend to develop active catalysts based on more abundant and cheaper materials.[5] In the past few decades, transition metal dichalcogenides (TMDs), represented as MX_2 (M = transition metals, X = S, Se, and Te), have become a type of promising candidate compound to replace traditional catalysts based on platinum. Among these TMDs, molybdenum disulfide (MoS_2) has been proven to be an attractive HER catalyst with high chemical stability and good electrocatalytic performance.[5–8] Compared with bulk MoS_2, a two-dimensional MoS_2 monolayer has better catalytic performance due to the exposure of a large fraction of active sites.[9,10] Several methods could further improve the catalytic activity of MoS_2, including choosing the Mo-edge of MoS_2 or introducing sulfur vacancy on the basal plane of MoS_2 as active sites.[11–16] In addition, some studies indicated that MoS_2 can also be used as a promising hydrogen storage material,[17] or as an excellent support[18] and catalyst[19–21] in the process of hydrogen storage. MoS_2-like nanostructures have also been widely studied for their high catalytic performance in hydrodesulfurization (HDS) of sulfur-containing compounds in fuels, and S–H groups were suggested to play an important role in supplying the hydrogen during HDS.[22,23] However, the morphology of MoS_2 nanoclusters in the catalyst is very complex, and the clusters on surfaces may have different shapes determined by the conditions under which they are synthesized.[22]

It is difficult to understand the reaction mechanism of catalytic reactions on the surface of molybdenum sulfide materials due to the complexity of real catalysts. However, clusters composed of limited number of atoms are experimentally and computationally tractable systems, so studies on rational cluster models may serve as a bottom-up strategy to understand complex systems and processes.[24,25] As for molybdenum sulfide clusters, the stable structures and properties of small stoichiometric $(MoS_2)_n$ clusters have been investigated.[26,27] Our previous work[27] reveals that the

[a] *School of Mathematics and Physics, North China Electric Power University, Beinong Road 2, Huilongguan, Beijing 102206, P. R. China. E-mail: dingxl@ncepu.edu.cn, djiaj@ncepu.edu.cn*
[b] *Institute of Clusters and Low Dimensional Nanomaterials, North China Electric Power University, Beinong Road 2, Huilongguan, Beijing 102206, P. R. China*
[c] *State Key Laboratory of Alternate Electrical Power System with Renewable Energy Sources, North China Electric Power University, Beijing 102206, China*
[d] *Beijing Key Laboratory of Energy Safety and Clean Utilization, North China Electric Power University, Beijing 102206, China*

† Electronic supplementary information (ESI) available: All data for Mo–Mo distances, natural bond orbital analysis for H_2...Mo_xS_y clusters, all obtained structures of Mo_xS_y clusters, the relationship between E_{ad} and other adsorption properties, and preliminary calculations on the grid structure. See DOI: 10.1039/d0cp04457a

structure of stoichiometric $(MoS_2)_n$ clusters can be viewed as fragments of the MoS_2 monolayer with the 1T phase, which implies a connection between the clusters and bulk phase materials. Considering that the high reactivity of molybdenum disulfide catalysts is mostly due to the edges or sulfur vacancies, it is of vital importance to research non-stoichiometric molybdenum sulfide clusters which are more suitable for simulating imperfect local structures of the surface or amorphous molybdenum sulfide than the stoichiometric ones. Some stable structures and properties of non-stoichiometric Mo_xS_y clusters have been obtained,[28–33] and other studies used these structures as models to study the adsorption or reaction for small molecules, such as H_2 and CO_2, to synthesize methanol. Different catalytic properties of stoichiometric and non-stoichiometric clusters have been found.[34] Baloglou *et al.*[24] studied the structures of $Mo_3S_{13}^{2-}$ and its protonated forms. They found that the H atoms prefer to make the S–H bond rather than the Mo–H bond in these S-rich clusters and suggested the "sulfur-centered" mechanism of HER catalysis. Recently, Raghavachari and Gupta *et al.*[35] investigated the adsorption and dissociation of the H_2 molecule on some anionic $Mo_xS_y^-$ clusters (x = 1, y = 3–5; x = 2, y = 2–4; x = 3, y = 3–5). They found that the formation of the Mo–H bond is preferred by not only S-deficient clusters (*e.g.*, $Mo_2S_2^-$) but also some S-rich clusters (*e.g.*, $Mo_2S_5^-$), while the H atom is more likely to combine with the S atom and finally form the H_2S molecule only for MoS_4^- and MoS_5^-, in which the only Mo atom is coordinated with four S atoms and has no coordination space for H or H_2. They also investigated the reactions of some anionic $Mo_xS_y^-$ with H_2O to reveal the mechanisms of the HER with cluster models.[36–38]

It is clear that different ratios of x to y influence the reaction mechanisms to a large extent, and the charge state of clusters may also have a significant impact on their reactivity. Since in previous work, much attention has been paid to anionic $Mo_xS_y^-$ clusters, a systematic study on neutral non-stoichiometric Mo_xS_y clusters is needed to obtain the comprehensive information of the structures of Mo_xS_y and the relationship with the reactivity towards H_2. Here, we report the structures of Mo_xS_y (x = 2–4; y = 2–10) clusters obtained by density functional theory (DFT) calculations. Based on that, we further discuss the adsorption and dissociation of H_2 on some typical clusters. The formation of the H_2 molecule from two H atoms on surfaces and the desorption of H_2 from the surface are two important steps in the HER. Our studies on the adsorption and dissociation of H_2 on clusters may be viewed as the reverse processes of the two steps, which may provide some useful information for understanding the mechanisms of the HER. The adsorption and dissociation processes studied in this work also have a close relationship with the fields of hydrogen storage and HDS.

Theoretical methods

All our DFT calculations were performed using the Gaussian 16 program suite.[39] A Fortran code based on a genetic algorithm and DFT calculations was developed[40] to generate sufficient and reasonable initial structures of Mo_xS_y clusters, which has also been successfully applied to some other clusters.[41–43] Then different isomers were optimized with the B3LYP hybrid density functional[44–46] and the def2-TZVP basis set.[47] The B3LYP functional was chosen since it has been adopted in some previous studies on Mo_xS_y clusters and provided reasonable results.[31,36,48,49] Dispersion correction[50] and diffuse functions[51] were involved in all calculations, which may be necessary for the reliable description of the interaction between H_2 and the clusters. Systems with Mo atoms may have complicated electronic states, so the singlet, triplet and quintet states were all taken into account in our calculations, as was done in previous work.[52,53] Electrostatic potential (ESP) analysis was performed to investigate the favorite adsorption site of Mo_xS_y for the hydrogen molecule. Natural bond orbital (NBO) analysis[54] was performed to acquire the electron transfer in the adsorption complexes and orbital interactions through second order perturbation theory. Harmonic vibrational frequency calculations were performed on optimized structures at the same theoretical level to ascertain the nature of the stationary points (no imaginary frequencies for minima and only one imaginary frequency for transition states). All energies reported in this work are total electronic energy with zero-point vibrational energy (ZPE) correction, except that the Gibbs free energy was reported for the dissociation reaction of H_2 on clusters. The Gibbs free energy was calculated with the standard temperature (298.15 K) and pressure (1 atm), which was commonly used in previous theoretical studies on the HER.[15,35,37,55,56]

Results and discussion

Structures of Mo_xS_y clusters (x = 2–4; y = 2–10)

The most stable and some typical low-lying isomers of Mo_xS_y clusters (x = 2–4; y = 2–10) are shown in Fig. 1. Considering the accuracy of calculation methods, the most stable structure under a certain theoretical level may not necessarily be the ground state of the cluster. In addition, the studied clusters are used to simulate the local structures on surfaces, and metastable structures of clusters may also exist on surfaces. Therefore, besides the most stable structure, we also provided several metastable structures of each cluster in this work (Fig. S1–S3 in the ESI†).

Most low-lying isomers tend to have singlet electronic states, and triplet is also quite common. Specifically, the most stable structures of the studied Mo_xS_y (denoted as ***x*–*y*a**) are all singlet, except that the triplet is preferred for $Mo_2S_{2,4,8}$, Mo_3S_3, and Mo_4S_9. For some clusters, the singlet and triplet have very close energies: the singlet of **3–7a**/**4–4a** is only 0.03/0.06 eV higher in energy than the corresponding triplet, while the singlet of **3–4a**/**4–8b** is more stable than the triplet by only 0.01/0.03 eV, respectively. Therefore, the ground states of these clusters could be either singlet or triplet. Quintet electronic states generally have higher energies than the singlets and triplets for all the obtained structures (as shown in Fig. 1 and Fig. S1–S3, ESI†), except **2–3b** and **4–9b**. For most clusters, ***x*–*y*a** is lower in energy than the corresponding second

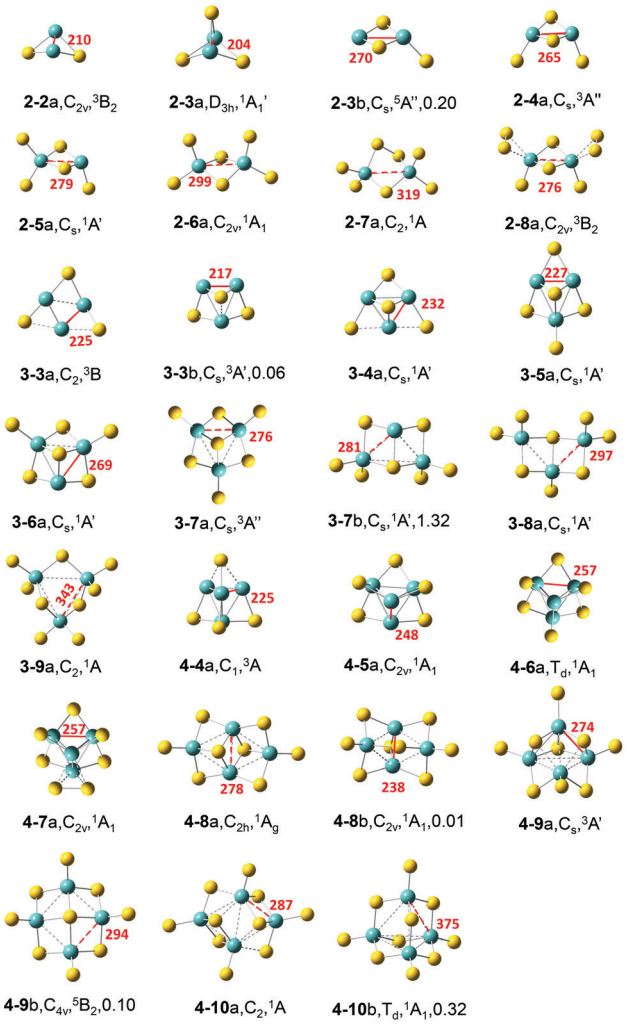

Fig. 1 Most stable and some typical low-lying isomers of Mo_xS_y clusters (x = 2–4; y = 2–10). Dashed lines denote the Mo–Mo bonds of 275–380 pm, Mo–S bonds of 244–275 pm, and S–S bonds of 214–237 pm. The symmetry, electronic state, and relative energy (in eV) with respect to the ground state are listed below each structure. The red line and number stand for the shortest distance between the two Mo atoms in each cluster.

most stable structure (denoted as ***x*–*y*b**) by more than about 0.2 eV, so it is quite reliable to assign that ***x*–*y*a** is the ground state structure for each cluster. There are three exceptions, Mo_3S_3, Mo_4S_8 and Mo_4S_9, for which the difference between ***x*–*y*a** and ***x*–*y*b** is less than 0.1 eV. So, for these clusters, the ***x*–*y*b** structures are also reliable candidates for ground state structures.

Below, we focus on the most stable structure of each cluster. When x = 2, an Mo_2-2S_B (S_B is for the bridging S) moiety with a rhombus structure is found in all of the most stable structures except **2–7a**. As y increases, the structures **2–3a**, **2–4a**, **2–5a**, and **2–6a** can be constructed from **2–2a** by adding one S_B, two, three, and four S_T (terminal S) atoms, respectively. **2–7a** can be viewed as **2–6a** with one Mo–S_B–Mo unit replaced by Mo–S–S–Mo. **2–8a** can be formed by **2–4a** with two S_2^{2-} ions. The Mo–Mo bond length (d_{Mo-Mo}) for the S-deficient Mo_2S_y clusters ($y < 2x$, here x = 2) is quite short (Table 1, 210 and 204 pm for y = 2 and 3, respectively), and it increases remarkably to 265 pm in

Table 1 Calculated average distance between Mo–Mo atoms ($\bar{d}$) in the most stable structure of Mo_xS_y clusters (Mo–Mo distances longer than 380 pm are ignored). All values are in picometer

	Mo_2S_y	Mo_3S_y	Mo_4S_y
y	$\bar{d}$	$\bar{d}$	$\bar{d}$
2	210		
3	204	244	
4	265	242	250
5	279	255	254
6	299	273	257
7	319	288	257
8	276	297	280
9		347	315
10			308

stoichiometric Mo_2S_4, while that for all the S-rich Mo_2S_y clusters ($y > 4$) is larger than 275 pm. Considering the values of the bond lengths in the bulk MoS_2 (275 pm for the 1T phase and 316 pm for the 2H phase[57]), the short d_{Mo-Mo} (shorter than 275 pm) values for S-deficient and stoichiometric Mo_2S_y clusters indicate that Mo–Mo interactions are strongly favored in these clusters. Short d_{Mo-Mo} in these clusters was suggested to have a close relationship with the high activity of amorphous and 1T phase MoS_2 in the HER.[57] The bonds with d_{Mo-Mo} between 275 and 380 pm (*ca.* 316 pm *1.2) indicate a medium interaction between the two Mo atoms (shown as dashed lines in Fig. 1), and all the calculated S-rich Mo_2S_y clusters have medium d_{Mo-Mo}.

For x = 3, an Mo_3 core capped with an S_F (S_F is for face-capping S) is favored in Mo_3S_{3-7}. **3–3b** with such an Mo_3–S_F moiety is higher in energy than **3–3a** by only 0.06 eV. **3–4a** can be obtained by **3–3a** with an additional S_F or by **3–3b** with an S_B. **3–5a**, **3–6a**, and **3–7a** can be constructed by adding one, two, and three S_T atoms to **3–4a**, respectively. The average distances between the Mo atoms ($\bar{d}$) as well as the shortest distances (d_1) gradually elongate as y increases from 3 to 9 (Table 1 and Fig. 1. Values for all the Mo–Mo distances are in Table S1 in the ESI†). S-deficient Mo_3S_y clusters have short d_{Mo-Mo}, while stoichiometric Mo_3S_6 has the d_{Mo-Mo} near to the experimental value of the bulk MoS_2 with the 1T phase. In **3–8a**, the Mo_3 core is broken with one Mo–Mo distance as large as 409 pm, and in **3–9a**, all the three Mo–Mo distances are longer than 340 pm.

For x = 4, a three-dimensional tetrahedron Mo_4 core is favored for the most stable structures of S-deficient Mo_4S_{4-7}. All the S atoms locate on the edges of the Mo_4 tetrahedron as S_B for y = 4–6, and **4–7a** can be viewed as **4–6a** with one S_B replaced by an S–S moiety. For the Mo_4 core, all the Mo–Mo distances are small (less than 259 pm) and the values of $\bar{d}$ gradually elongate from 250 to 257 pm as y increases from 4 to 7. The Mo_4 core does not exist in the most stable structures of stoichiometric Mo_4S_8 and S-rich $Mo_4S_{9,10}$ clusters. In the 1T-phase structure of the stoichiometric **4–8a**, four Mo atoms form a rhombus structure with $\bar{d}$ being 280 pm. **4–9a** has a distorted tetrahedral Mo_4 whose Mo–Mo distances are much longer than those in S-deficient Mo_4S_{4-7}, and on it there are two S_B, three S_F, and four S_T atoms. In **4–10a** four Mo atoms form a rhombus structure, similar to **4–8a** but with longer $\bar{d}$, and there are two S_F, four S_B, and four S_T atoms.

In all stable geometric structures shown in Fig. 1 (and also those in Fig. S1–S3, ESI†), the oxidation state of each Mo atom is no more than +6, if we roughly assume that each S_T on the Mo atom contributes +2, while each S_B contributes +1. This is consistent with that each Mo atom has 6 valence electrons. Mo atoms with the +6 oxidation state first appear in S-rich clusters **2–5a** and **3–9a** (also **4–10c** in Fig. S3, ESI†). As for the coordination of Mo atoms, it is found that each Mo tends to have bonds with at most four S atoms in the studied clusters, with only a few exceptions in which the coordination number of Mo is five (*e.g.*, **2–8a** and **4–9a**), while for the bulk materials, each Mo atom is coordinated with six S_F atoms in both the 1T and 2H phase monolayers.

Gemming *et al.* studied the structures of Mo_xS_y clusters (x = 1 and 2, y = 1–6; and x = 4, y = 1–12)[31] and anionic $Mo_3S_y^-$ (y = 0–12).[33] Our calculations with different basis sets confirm their findings for Mo_xS_y (x = 2, y = 2–6; x = 4, y = 4–10) and provide more low-lying structures for each cluster. Moreover, their structure for Mo_4S_8 is actually **4–8b** in our calculations which is slightly higher in energy than **4–8a** by 0.01 eV. They suggested that **4–6a** with a high symmetry (T_d) is a magic cluser with extraordinarily high stability according to its relatively high average binding energy of S atoms among $Mo_4S_y^-$ (y = 1–10) clusters. Our calculations further confirm that **4–6a** is very stable since the energy difference between **4–6a** and **4–6b** is as large as 3.34 eV. Additionally, isomer **4–10b** also has T_d symmetry, and its structure is the same as that of V_4O_{10}, which has many interesting properties.[58,59]

In our previous work,[27] the most stable structures and some low-lying structures for $(MoS_2)_n$ (n = 1–6) have been obtained by using B3LYP and PW91 functionals with def2-TZVP basis sets. A type of structure that can be viewed as fragments of monolayer MoS_2 with the 1T phase was found in these stoichiometric $(MoS_2)_n$ clusters. In this work, after including dispersion correction and adding diffuse functions to the basis sets, similar results are obtained for the clusters studied in both studies (*i.e.*, Mo_2S_4, Mo_3S_6, and Mo_4S_8), which further confirmed the reliability of the theoretical level we used in both studies. In this work, we find that the 1T-type structure found in stoichiometric $(MoS_2)_n$ clusters also exists in non-stoichiometric clusters, such as **3–7a**. Additionally, we find another type of structure, as in **3–7b**, **3–8a**, and **4–9b**, which has a regular bonding mode with square Mo_2S_2 units, and all the Mo atoms are well separated by S atoms. The distance between the two Mo atoms in the square Mo_2S_2 unit is longer than 280 pm, even longer than the Mo–Mo distance in the 1T phase MoS_2 monolayer. We speculate that this grid structure might be used as a building-block to construct a new type of two-dimensional molybdenum sulfide monolayer, in which four-coordinated S atoms exist as in **4–9b**. Preliminary calculations with a two-dimensional periodic slab model, including zone centered (Γ-point) vibrational frequencies and *ab initio* molecular dynamics calculations, show that this type of grid structure is quite stable under room temperature (detailed calculation results are in the ESI†). Further investigations on this novel structure are required to verify the stability and reveal more unique properties.

Adsorption of the H_2 molecule on Mo_xS_y clusters

Adsorption of the H_2 molecule on the most stable Mo_xS_y clusters was studied with different adsorption sites and possible spin multiplicities. For clusters **3–3**, **4–8**, and **4–9**, two low-lying isomers (a and b) were calculated since they are both considered as candidates for the most stable structures. Seventeen adsorption complexes with relatively large adsorption energy (will be described clearly later) have been obtained (Fig. 2). The symbol H_2-***xy*a(b)** stands for the adsorption complex of H_2 on ***x*–*y*a(b)**. For H_2-**33b**, H_2-**45a**, and H_2-**47a**, two different adsorption sites have been found, and the second one is labelled with an apostrophe (′). Spin multiplicities do not change after the adsorption of H_2, except that for **3–4a**, the singlet is more stable than the triplet by 0.01 eV before adsorption, while the triplet is lower in energy by 0.10 eV for H_2-**34a**. In these clusters, H_2 is adsorbed on Mo atoms with the oxidation state not exceeding +4, which is similar to the results of the H_2 adsorption on anionic $Mo_xS_y^-$ clusters.[35] Xu *et al.*[10] revealed that S vacancies in two dimensional MoS_2 would contribute to a significant enhancement of the HER performance. It is clear that the S vacancy in the bulk phase MoS_2 could cause the oxidation state of Mo being less than +4, leading to easy adsorption of H_2, which is consistent with our findings.

Several properties are used to evaluate the strength of the interaction between H_2 and Mo_xS_y clusters (Table 2). E_{ad} is a

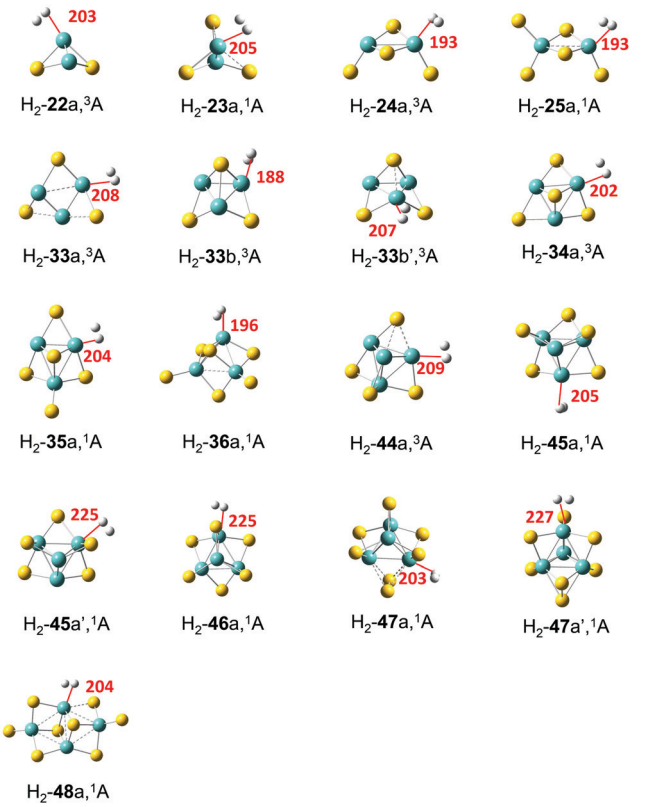

Fig. 2 Stable geometric structures of H_2 adsorption on Mo_xS_y clusters with an adsorption energy larger than 0.1 eV. The red line and the number stand for the shorter distance (d_{H-Mo}, in pm) between two H atoms and Mo for each adsorption system.

Table 2 Properties for the adsorption of H_2 on Mo_xS_y clusters. Listed are adsorption energy (E_{ad}, in eV), free energy change (ΔG, in kcal mol^{-1}) at 298.15 K, electron transfer from Mo_xS_y to H_2 by natural population analysis (Q, in $|e|$), bond length (in pm) of H–Mo (d_{H-Mo}) and H–H (d_{H-H}), symmetric (ν_s(Mo–H_2)) and asymmetric (ν_a(Mo–H_2)) vibration between H_2 and Mo, and vibration of H–H (ν(H–H)). Values of d_{H-H} and ν(H–H) for free H_2 are also listed for comparison (in cm^{-1})

Clusters	E_{ad}	ΔG	Q	d_{H-Mo}	d_{H-H}	ν_s(Mo–H_2)	ν_a(Mo–H_2)	ν(H–H)
H_2					74			4418
H_2-**22a**	0.25	0.61	0.14	203	79	716	1242	3628
H_2-**23a**	0.12	3.15	0.18	205	78	668	1214	3761
H_2-**24a**	0.49	−4.54	0.27	193	81	867	1440	3336
H_2-**25a**	0.40	−2.47	0.25	193	81	839	1441	3372
H_2-**33a**	0.16	2.09	0.17	208	78	611	1107	3823
H_2-**33b**	0.47	−4.22	0.22	188	85	892	1571	2800
H_2-**33b′**	0.28	−0.51	0.19	207	78	667	1077	3770
H_2-**34a**	0.33	−1.81	0.35	202	78	733	1213	3747
H_2-**35a**	0.21	1.93	0.27	204	78	699	1235	3816
H_2-**36a**	0.31	−0.75	0.24	196	80	1011	1400	3443
H_2-**44a**	0.28	0.15	0.19	209	77	636	1082	3883
H_2-**45a**	0.30	−0.77	0.25	205	78	676	1150	3805
H_2-**45a′**	0.13	2.92	0.24	225	77	3121	994	4152
H_2-**46a**	0.13	1.40	0.23	225	76	2933	972	4136
H_2-**47a**	0.34	−1.45	0.32	203	78	722	1192	3862
H_2-**47a′**	0.12	3.19	0.22	227	76	2866	969	4128
H_2-**48a**	0.16	3.57	0.28	204	78	687	1224	3858

direct measure of the strength, which is defined as $E_{ad} = E(H_2) + E(Mo_xS_y) - E(H_2 - Mo_xS_y)$. Note that in the calculation of E_{ad} for systems like H_2-**33b**, the energy of **3–3b** (not the more stable **3–3a**) is used for $E(Mo_xS_y)$. All the Mo_xS_y clusters with the ratio of x to y no more than 1 : 2 can adsorb H_2 with an adsorption energy larger than 0.1 eV, while all the S-rich clusters cannot adsorb H_2 except Mo_2S_5. It was suggested that the binding energy of hydrogen to an ideal hydrogen storage material should be intermediate between physisorption and chemisorption, about 0.2–1.0 eV.[60] For the listed clusters in Fig. 2, E_{ad} ranges from 0.12 to 0.49 eV (H_2-**24a** has the highest E_{ad}), indicating that molybdenum sulfide may be acceptable hydrogen storage materials for some special occasions.

Kubas[61] found that when H_2 is bound to a transition metal atom, electrons will transfer from the hydrogen molecule to the unfilled d-orbital of the transition metal atom with back-donation of electrons from the transition metal to the anti-bonding orbitals of H_2. In Table 2, the electron transfer from H_2 to the cluster (Q) is listed. For all clusters, Q is positive and ranges from 0.14 $|e|$ for H_2-**22a** to 0.35 $|e|$ for H_2-**34a**. However, the amount of Q does not have a clear relationship with E_{ad} (Fig. S4 in the ESI†). Further NBO analysis on interactions between the filled donor and empty acceptor NBOs of the adsorption complexes estimates the energetic importance of these interactions through second order perturbation theory. The results (Table S2 in the ESI†) indicate that the dominant interaction is the H–H bond as the donor NBO and the Mo–Mo or Mo–S anti-bond as the acceptor with a high second-order perturbation energy (ΔE_2, also be termed as the donor–acceptor orbital interaction stabilization energy) while the back-donation with the lone-pair Mo NBO as the donor and the H–H anti-bond as the acceptor usually has low values of ΔE_2 in most adsorption systems.

From the geometric point of view, when H_2 is adsorbed on an Mo atom in Mo_xS_y clusters, the distance between H_2 and Mo can be another indicator of the strength of adsorption. The H_2 molecule is always side-on adsorbed on one Mo atom, and the short one of the distances between Mo and the two H atoms is denoted as d_{H-Mo} (Fig. 2 and Table 2). It is clear that d_{H-Mo} is closely related to E_{ad} (Fig. S5 in the ESI†): three adsorption complexes with the shortest d_{H-Mo} ($\leq$193 pm for H_2-**24a**, **25a**, and **33b**) have the highest E_{ad} ($\geq$0.40 eV), while three complexes with the longest d_{H-Mo} ($\geq$225 pm for H_2-**45a′**, **46a**, and **47a′**) all have very small E_{ad} ($\leq$0.13 eV). Another geometric parameter is the bond length of H–H (d_{H-H}). Considering the charge transfer mechanism of H_2 adsorption, it is expected that stronger adsorption will lead to longer d_{H-H}. Our results (Fig. S6 in the ESI,† or Table 2) generally agree with this expectation. Compared with the d_{H-H} of the free H_2 molecule (74 pm), the d_{H-H} is lengthened significantly ($\geq$81 pm) in three complexes with the highest E_{ad} (H_2-**24a**, **25a**, **33b**), indicating that H_2 in these complexes is activated to some extent.

Vibrational frequencies of adsorption complexes are useful information to identify the structures of different adsorption sites when compared with Fourier transform infrared (FTIR) or Raman experiments. Three vibrational modes have been found associated with H_2 for each adsorption complex, namely, the symmetric vibration between Mo and H_2 (ν_s(Mo–H_2)), in which two H atoms move in the same direction to Mo, the asymmetric one (ν_a(Mo–H_2)), in which two H atoms move in the opposite direction to Mo, and the stretch vibration of the H–H bond (ν(H–H)). High values of ν_s(Mo–H_2) and ν_a(Mo–H_2) generally indicate higher interaction strength between H_2 and the clusters (Fig. S7 and S8 in the ESI,† or Table 2). Three complexes with the longest d_{H-Mo} (H_2-**45a′**, **46a**, **47a′**) are exceptions – they have extremely high values of ν_s(Mo–H_2), even larger than 2850 cm^{-1}, while their interactions with the clusters are very small (*e.g.*, with very small E_{ad}). Upon adsorption, the H–H bond will be weakened, leading to a decrease of ν(H–H)

values in the adsorption complexes, and larger E_{ad} may cause smaller ν(H–H) in general (Fig. S9 in the ESI,† or Table 2). Specifically, H_2-**33b** has the smallest value (2800 cm^{-1}) of ν(H–H), which is much smaller than the free H_2 (4418 cm^{-1}). H_2-**33b** has the smallest value for ν(H–H) and the largest value for d(H–H), indicating the greatest extent of H_2 activation on it; H_2-**33b** also has the shortest d_{H-Mo} and the largest ν_a(Mo–H_2), which corresponds to the strong interaction between H_2 and clusters. Note that the total energy of H_2-**33b** is lower than that of H_2-**33a**, although **3–3a** is more stable than **3–3b**, which further implies that H_2-**33b** is very stable and the adsorption capacity of **3–3b** is particularly strong.

The electric field produced by metal cations can polarize the H_2 molecule and enhance the binding of H_2 on metal atoms.[62] For the clusters studied in this work, different adsorption sites may have a distinct ability to polarize H_2, leading to the variation of the adsorption strength. To investigate the polarization ability of Mo_xS_y clusters, the molecule surface electrostatic potentials (ESPs) of typical clusters (**3–3b**, **4–4a**, **4–5a**, and **4–7a**) are calculated and shown in Fig. 3. The local maximum values of the ESP (V_{max})[63,64] are also listed. There are two types of Mo atoms in **3–3b**: the one with one S_B and one S_F has V_{max} = 2.67 V nearby (denoted as Mo_I), and the one with two S_B and one S_F has V_{max} = 1.56 V (Mo_II). H_2 adsorption on Mo_I corresponds to H_2-**33b**, while H_2 on Mo_II corresponds to H_2-**33b′**. All the properties discussed above (Table 2) indicate that the adsorption of H_2 in H_2-**33b** is much stronger than that in H_2-**33b′** (*e.g.*, E_{ad} is 0.47 and 0.28 eV, respectively). In addition, for each cluster shown in Fig. 3, the larger E_{ad} is always accompanied by the higher V_{max} for different adsorption sites. Mo atoms with less coordination (lower oxidation state) tend to have higher V_{max}. Therefore, they have a higher ability to adsorb the H_2 molecule.

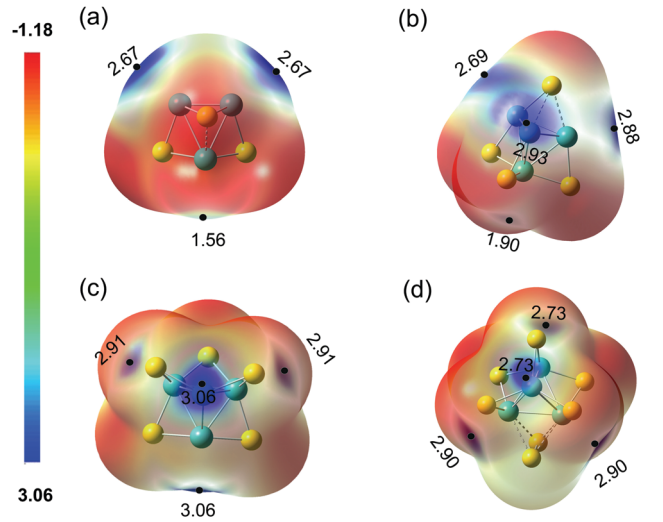

Fig. 3 Electrostatic potential calculated at the B3LYP-D3/ma-def2-TZVP level on the 0.001 au molecular surface of (a) Mo_3S_3, (b) Mo_4S_4, (c) Mo_4S_5, and (d) Mo_4S_7. The local maximum values of the electrostatic potential (V) for different active sites of the clusters were marked in the corresponding position.

Dissociation of H_2 on Mo_2S_4 and Mo_3S_3

Dissociation of H_2 was studied on the selected Mo_xS_y clusters. For comparing the results with those obtained by other research groups[6,35] more conveniently, we used Gibbs free energy in this section. The adsorption of H_2 on clusters would cause a decrease in the entropy and an increase of the Gibbs free energy of the system, and the increased value was estimated to be about 0.26 eV under room temperature.[65] So systems with small values of E_{ad} (Table 2) may be unstable under thermal conditions. The free energy change (ΔG) for the adsorption process is listed in Table 2. H_2-**24a** (stoichiometric) and H_2-**33b** (non-stoichiometric) have the most negative values of ΔG. Therefore, they were selected as two typical adsorption systems for investigation of the dissociation of H_2 on Mo_xS_y clusters. Both singlet and triplet states were calculated along the reaction paths since spin-crossover was found to occur commonly during these reactions,[66,67] although the ground states of **2–4a** and **3–3b** are both triplet. The sum of the free energies of infinite separated H_2 and triplet **2–4a** or **3–3b** was set to zero, respectively.

Fig. 4(a) shows the reaction path of **2–4a** with H_2. It starts from the triplet **2–4a** (lower in energy than ^{1}**2–4a** by 9.7 kcal mol^{-1})

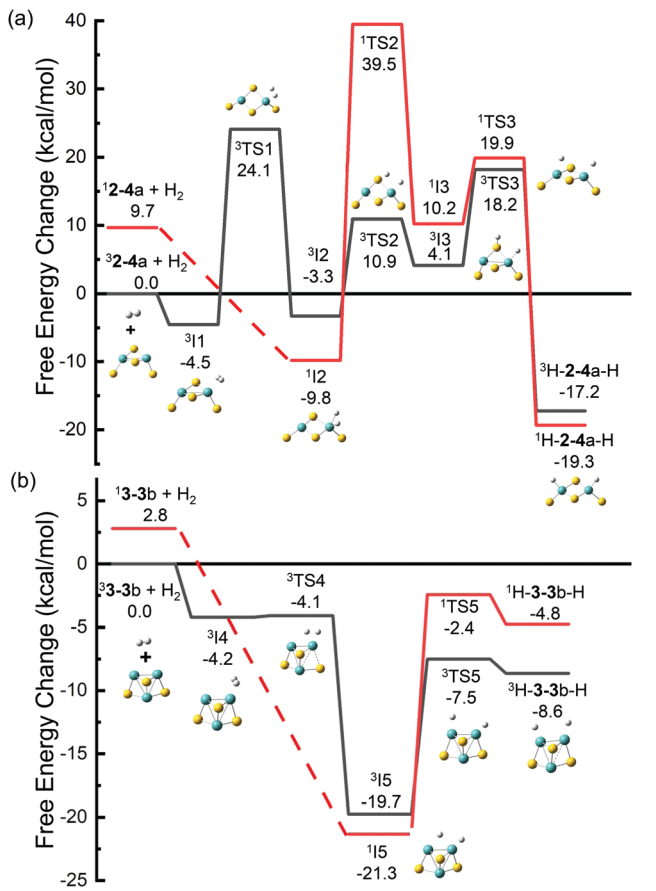

Fig. 4 DFT calculated potential energy profiles for the dissociation of H_2 on (a) Mo_2S_4 and (b) Mo_3S_3. Relative Gibbs free energies of the reaction intermediates (I1–I5), transition states (TS1–TS5), and products with respect to the separated reactants are given in kcal mol^{-1}.

and forms ^{3}I1 with −4.5 kcal mol^{-1} after adsorption. Then the H–H bond in ^{3}I1 (d_{H-H} = 81 pm) breaks, forming ^{3}I2 (−3.3 kcal mol^{-1}, and d_{H-H} = 177 pm) with a high energy barrier of 24.1 kcal mol^{-1}, or ^{1}I2 (−9.8 kcal mol^{-1}) through a spin-crossover. ^{1}I2 is energetically more favorable than ^{3}I2, and it can also be obtained directly from the adsorption of H_2 on singlet **2–4a** without any energy barriers. From ^{1}I2, one H atom may transfer to a neighboring S atom to form ^{1}I3 or ^{3}I3. The barrier is very high (39.5 kcal mol^{-1}) along the path with the singlet state. The path from ^{1}I2 to ^{3}I3 with a spin-crossover is more favorable, but it still has an overall barrier (10.9 kcal mol^{-1}), and ^{3}I3 has a positive relative energy. The H atom on S in ^{3}I3 tends to transfer to the other Mo atom to form ^{1}H-**2–4a**-H or ^{3}H-**2–4a**-H. Although these products are lower in energy than ^{1}I2, they actually cannot be formed in reactions of H_2 with **2–4a** considering the high energy barriers from ^{1}I2 to them. Recently, Gupta *et al.* studied the dissociation of H_2 on anionic $Mo_2S_4^-$,[35] and our results on neutral Mo_2S_4 have many similarities to theirs. Both neutral and anionic systems start with high spin multiplicity (triplet and quartet for neutral and anionic clusters, respectively) which is lower in energy, while low spin multiplicity is preferred for the dissociative adsorption of H_2 on one Mo atom (*e.g.*, ^{1}I2 in this work). The low spin state isomers with two H atoms adsorbed separately on different Mo atoms are found to be the most stable intermediates for both charge states. The only difference is that for a neutral system, there exists a stable adsorption isomer (^{3}I1) in which H_2 is not dissociated, which may be a favorable factor for H_2 adsorption in the initial stage.

Different situations are found for H_2 on **3–3b**, whose ground state is also a triplet (Fig. 4(b)). H_2 can be adsorbed on one Mo atom to form ^{3}I4, but ^{3}I4 is not stable and it can transform to a much more stable isomer (^{3}I5) with a negligible barrier (^{3}TS4, 0.1 kcal mol^{-1} with respect to ^{3}I4). The singlet ^{1}I5, which could be obtained directly from **3–3b** or from ^{3}I4 through a spin-crossover, is even more stable than ^{3}I5, but the energy difference is only 1.6 kcal mol^{-1}. ^{1}I5 and ^{3}I5 are the most stable intermediates for H_2 on **3–3b**, in which H_2 is dissociated with one H on an Mo atom and the other one on the bridge site of Mo–Mo. The bridging bonded H atom can move to the other Mo atom to form H-**3–3b**-H (two H atoms adsorbed on different Mo atoms). The relative energies of all isomers and transition states are less than zero, indicating that the transformation of H_2 on **3–3b** is much easier than that on **2–4a**.

For **3–3b**, the vacant bridge site of Mo–Mo is a favorite site for H atom adsorption (see ^{1}I5 and ^{3}I5 with very low relative energy), and the H atom can be transferred between the two Mo atoms through this bridge site easily (a bridge for H atom transfer). On the other hand, the bridge sites in **2–4a** have been occupied by S atoms, leading to the difficulty in the H atom transfer on **2–4a**. The vacant Mo–Mo bridge site corresponds to the S vacancy in the bulk phase MoS_2, and the dissociation reaction could be viewed as the reverse process of the HER. Therefore, our findings that **3–3b** with a vacant Mo–Mo bridge site has lower barriers for both H_2 dissociation and the HER are consistent with previous studies on the bulk phase MoS_2 in which promising electrocatalysts for the HER can be obtained by increasing the number of S vacancies in MoS_2.[68,69] Our results also indicate that H atoms prefer to be bound to Mo atoms rather than S atoms, which may be another aspect to understand the previous study that monolayer MoS_2 with the Mo edge is more likely to adsorb H atoms and realize the HER.[11,12]

Conclusions

The geometric and electronic properties of non-stoichiometric neutral Mo_xS_y clusters (x = 2–4; y = 2–10) for the most stable structures and low-lying isomers, together with the adsorption and dissociation of the H_2 molecule on selected clusters, were systematically studied by DFT calculations. In the S-deficient clusters, Mo atoms are more likely to come together and form an Mo_x core. Structures like the bulk 1T phase could be seen not only in stoichiometric clusters but also in non-stoichiometric Mo_xS_y clusters. Another type of structure with square Mo_2S_2 units was found, which might be a new primary unit for two-dimensional molybdenum sulfides. The hydrogen molecule prefers to be adsorbed onto Mo atoms rather than S atoms, and Mo atoms with less coordination of S tend to have a higher local ESP and higher ability to adsorb H_2. Among the studied clusters, **2–4a** and **3–3b** have the highest H_2 adsorption energy, on which the H_2 molecule is significantly activated. As a reverse reaction of HER, the dissociation of H_2 on **2–4a** and **3–3b** was studied. Hydrogen atoms are found to be adsorbed onto Mo atoms rather than S atoms, especially on the vacant *bridge* site of Mo–Mo in **3–3b**, which could be seen as the S vacancy in the bulk phase MoS_2. The bridge site of Mo–Mo facilitates the transfer of H atoms on Mo_xS_y clusters, indicating that S vacancies and Mo-edges in the bulk MoS_2 are beneficial for both H_2 dissociation and the HER. The H atom adsorbed on the bridge site of Mo–Mo may serve as another way to supply hydrogen in HDS, which may be verified by further investigations.

Conflicts of interest

There are no conflicts to declare.

Acknowledgements

This work was supported by the National Natural Science Foundation of China (No. 91545122 and No. 61704054), the Fundamental Research Funds for the Central Universities (JB2015RCY03, JB2019MS052, and JB2017MS056) supported by the fund of North China Electric Power University, and the National Key Research and Development Program of China (2016YFA0202401).

Notes and references

1 Z. W. Seh, J. Kibsgaard, C. F. Dickens, I. B. Chorkendorff, J. K. Norskov and T. F. Jaramillo, *Science*, 2017, **355**, eaad4998.
2 S. Chu, Y. Cui and N. Liu, *Nat. Mater.*, 2017, **16**, 16.

3 X. L. Wang, Y. J. Tang, W. Huang, C. H. Liu, L. Z. Dong, S. L. Li and Y. Q. Lan, *ChemSusChem*, 2017, **10**, 2402.
4 X. X. Zou and Y. Zhang, *Chem. Soc. Rev.*, 2015, **44**, 5148.
5 D. Voiry, J. Yang and M. Chhowalla, *Adv. Mater.*, 2016, **28**, 6197.
6 X. L. Wang, C. Z. Xue, N. N. Kong, Z. Wu, J. X. Zhang, X. Wang, R. Zhou, H. P. Lin, Y. Y. Li, D. S. Li and T. Wu, *Inorg. Chem.*, 2019, **58**, 12415.
7 J. S. Wang, J. Liu, B. Zhang, X. Ji, K. Xu, C. Chen, L. Miao and J. J. Jiang, *Phys. Chem. Chem. Phys.*, 2017, **19**, 10125.
8 J. Kang, S. Tongay, Z. Jian, J. Li and J. Wu, *Appl. Phys. Lett.*, 2013, **102**, 012111.
9 M.-R. Gao, M. K. Y. Chan and Y. Sun, *Nat. Commun.*, 2015, **6**, 7493.
10 Y. Xu, L. Wang, L. Xia, S. Zhang, C. Liu, D. Yan, Y. Zeng, P. Yong, Y. Liu and S. L. Luo, *J. Mater. Chem. A*, 2016, **4**, 16524.
11 T. F. Jaramillo, K. P. Jorgensen, J. Bonde, J. H. Nielsen, S. Horch and I. Chorkendorff, *Science*, 2007, **317**, 100.
12 K. K. Ghuman, S. Yadav and C. V. Singh, *J. Phys. Chem. C*, 2015, **119**, 6518.
13 A. Y. Lu, X. L. Yang, C. C. Tseng, S. X. Min, S. H. Lin, C. L. Hsu, H. N. Li, H. C. Idriss, J. L. Kuo, K. W. Huang and L. J. Li, *Small*, 2016, **12**, 5530.
14 L. X. Lin, N. H. Miao, Y. Wen, S. W. Zhang, P. Ghosez, Z. M. Sun and D. A. Allwood, *ACS Nano*, 2016, **10**, 8929.
15 H. Li, C. Tsai, A. L. Koh, L. Cai, A. W. Contryman, A. H. Fragapane, J. Zhao, H. S. Han, H. C. Manoharan, F. Abild-Pedersen, J. K. Nørskov and X. Zheng, *Nat. Mater.*, 2015, **15**, 364.
16 C. Tsai, H. Li, S. Park, J. Park, H. S. Han, J. K. Norskov, X. L. Zheng and F. Abild-Pedersen, *Nat. Commun.*, 2017, **8**, 15113.
17 J. Chen, N. Kuriyama, H. Yuan, H. T. Takeshita and T. Sakai, *J. Am. Chem. Soc.*, 2001, **123**, 11813.
18 N. H. Song, Y. S. Wang, H. Y. Gao, W. F. Jiang, J. Zhang, B. Xu, Q. Sun and Y. Jia, *Phys. Lett. A*, 2015, **379**, 815.
19 Z. M. Yuan, B. W. Zhang, Y. H. Zhang, S. H. Guo, X. P. Dong and D. L. Zhao, *J. Mater. Sci. Technol.*, 2018, **34**, 1851.
20 E. J. Setijadi, X. Li, A. F. Masters, T. Maschmeyer and K.-F. Aguey-Zinsou, *Int. J. Hydrogen Energy*, 2016, **41**, 3551.
21 Y. H. Jia, S. M. Han, W. Zhang, X. Zhao, P. F. Sun, Y. Q. Liu, H. Shi and J. S. Wang, *Int. J. Hydrogen Energy*, 2013, **38**, 2352.
22 J. V. Lauritsen, M. V. Bollinger, E. Laegsgaard, K. W. Jacobsen, J. K. Norskov, B. S. Clausen, H. Topsoe and F. Besenbacher, *J. Catal.*, 2004, **221**, 510.
23 P. G. Moses, B. Hinnemann, H. Topsoe and J. K. Norskov, *J. Catal.*, 2007, **248**, 188.
24 A. Baloglou, M. Oncak, M. L. Grutza, C. van der Linde, P. Kurz and M. K. Beyer, *J. Phys. Chem. C*, 2019, **123**, 8177.
25 Q. Y. Liu and S. G. He, *Chem. J. Chin. Univ.-Chin.*, 2014, **35**, 665.
26 P. Murugan, V. Kumar, Y. Kawazoe and N. Ota, *Phys. Rev. A: At., Mol., Opt. Phys.*, 2005, **71**, 063203.
27 Y. Y. Wang, J. J. Deng, X. Wang, J. T. Che and X. L. Ding, *Phys. Chem. Chem. Phys.*, 2018, **20**, 6365.
28 H. Jiao, Y.-W. Li, B. Delmon and J.-F. Halet, *J. Am. Chem. Soc.*, 2001, **123**, 7334.
29 X. Zhang, X. Liu, R. Xu, N. Wu, X. Huang and B. Wang, *Chin. J. Struct. Chem.*, 2018, **37**, 497.
30 M. Ziane, F. Amitouche, S. Bouarab and A. Vega, *J. Nanopart. Res.*, 2017, **19**, 380.
31 S. Gemming, J. Tamuliene, G. Seifert, N. Bertram, Y. D. Kim and G. Gantefor, *Appl. Phys. A: Mater. Sci. Process.*, 2006, **82**, 161.
32 N. Bertram, Y. D. Kim, G. Gantefor, Q. Sun, P. Jena, J. Tamuliene and G. Seifert, *Chem. Phys. Lett.*, 2004, **396**, 341.
33 S. Gemming, G. Seifert, M. Götz, T. Fischer and G. Ganteför, *Phys. Status Solidi B*, 2010, **247**, 1069.
34 P. Liu, Y. Choi, Y. X. Yang and M. G. White, *J. Phys. Chem. A*, 2010, **114**, 3888.
35 A. K. Gupta, J. E. Topolski, K. A. Nickson, C. C. Jarrold and K. Raghavachari, *J. Phys. Chem. A*, 2019, **123**, 7261.
36 N. J. Mayhall, E. L. Becher, A. Chowdhury and K. Raghavachari, *J. Phys. Chem. A*, 2011, **115**, 2291.
37 J. E. Topolski, A. K. Gupta, K. A. Nickson, K. Raghavachari and C. C. Jarrold, *Int. J. Mass Spectrom.*, 2018, **434**, 193.
38 A. Saha and K. Raghavachari, *J. Chem. Phys.*, 2013, **139**, 12.
39 M. J. Frisch, G. W. Trucks, H. B. Schlegel, G. E. Scuseria, M. A. Robb, J. R. Cheeseman, G. Scalmani, V. Barone, G. A. Petersson, H. Nakatsuji, X. Li, M. Caricato, A. V. Marenich, J. Bloino, B. G. Janesko, R. Gomperts, B. Mennucci, H. P. Hratchian, J. V. Ortiz, A. F. Izmaylov, J. L. Sonnenberg, D. Williams-Young, F. Ding, F. Lipparini, F. Egidi, J. Goings, B. Peng, A. Petrone, T. Henderson, D. Ranasinghe, V. G. Zakrzewski, J. Gao, N. Rega, G. Zheng, W. Liang, M. Hada, M. Ehara, K. Toyota, R. Fukuda, J. Hasegawa, M. Ishida, T. Nakajima, Y. Honda, O. Kitao, H. Nakai, T. Vreven, K. Throssell, J. A. Montgomery, Jr., J. E. Peralta, F. Ogliaro, M. J. Bearpark, J. J. Heyd, E. N. Brothers, K. N. Kudin, V. N. Staroverov, T. A. Keith, R. Kobayashi, J. Normand, K. Raghavachari, A. P. Rendell, J. C. Burant, S. S. Iyengar, J. Tomasi, M. Cossi, J. M. Millam, M. Klene, C. Adamo, R. Cammi, J. W. Ochterski, R. L. Martin, K. Morokuma, O. Farkas, J. B. Foresman and D. J. Fox, *Gaussian 16, Rev. A.03*, Gaussian Inc, Wallingford, CT, 2016.
40 X. L. Ding, Z. Y. Li, J. H. Meng, Y. X. Zhao and S. G. He, *J. Chem. Phys.*, 2012, **137**, 214311.
41 L. F. Li and L. J. Cheng, *J. Chem. Phys.*, 2013, **138**, 094312.
42 X. N. Li, L. N. Wang, L. H. Mou and S. G. He, *J. Phys. Chem. A*, 2019, **123**, 9257.
43 X. L. Ding, D. Wang, R. J. Li, H. L. Liao, Y. Zhang and H. Y. Zhang, *Phys. Chem. Chem. Phys.*, 2016, **18**, 9497.
44 A. D. Becke, *Phys. Rev. A: At., Mol., Opt. Phys.*, 1988, **38**, 3098.
45 A. D. Becke, *J. Chem. Phys.*, 1993, **98**, 5648.
46 C. Lee, W. Yang and R. G. Parr, *Phys. Rev. B: Condens. Matter Mater. Phys.*, 1988, **37**, 785.
47 F. Weigend and R. Ahlrichs, *Phys. Chem. Chem. Phys.*, 2005, **7**, 3297.
48 B. Liang and L. Andrews, *J. Phys. Chem. A*, 2002, **106**, 6295.
49 B. Wang, N. Wu, X. B. Zhang, X. Huang, Y. F. Zhang, W. K. Chen and K. N. Ding, *J. Phys. Chem. A*, 2013, **117**, 5632.
50 S. Grimme, J. Antony, S. Ehrlich and H. Krieg, *J. Chem. Phys.*, 2010, **132**, 154104.

51 J. Zheng, X. Xu and D. G. Truhlar, *Theor. Chem. Acc.*, 2011, **128**, 295.
52 N. Bridonneau, J. Long, J. L. Cantin, J. von Bardeleben, S. Pillet, E. E. Bendeif, D. Aravena, E. Ruiz and V. Marvaud, *Chem. Commun.*, 2015, **51**, 8229.
53 B. Bishnoi and B. Ghosh, *J. Comput. Electron.*, 2014, **13**, 394.
54 E. D. Glendening, J. K. Badenhoop, A. E. Reed, J. E. Carpenter, J. A. Bohmann, C. M. Morales, C. R. Landis and F. Weinhold, *NBO 6.0.*, Madison, WI, Theoretical Chemistry Institute, University of Wisconsin, 2013.
55 P. Xiao, W. Chen and X. Wang, *Adv. Energy Mater.*, 2015, **5**, 1500985.
56 J. K. Norskov, T. Bligaard, A. Logadottir, J. R. Kitchin, J. G. Chen, S. Pandelov and U. Stimming, *J. Electrochem. Soc.*, 2005, **152**, J23.
57 L. Wu, A. Longo, N. Y. Dzade, A. Sharma, M. Hendrix, A. A. Bol, N. H. de Leeuw, E. J. M. Hensen and J. P. Hofmann, *ChemSusChem*, 2019, **12**, 4383.
58 N. Kaur, I. Kumari, S. Gupta and N. Goel, *J. Phys. Chem. A*, 2016, **120**, 9588.
59 J. B. Ma, X. N. Wu, X. X. Zhao, X. L. Ding and S. G. He, *Phys. Chem. Chem. Phys.*, 2010, **12**, 12223.
60 P. Jena and Q. Sun, *Chem. Rev.*, 2018, **118**, 5755.
61 G. J. Kubas, *Acc. Chem. Res.*, 1988, **21**, 120.
62 J. Niu, B. K. Rao and P. Jena, *Phys. Rev. Lett.*, 1992, **68**, 2277.
63 T. Lu and F. W. Chen, *J. Comput. Chem.*, 2012, **33**, 580.
64 T. Lu and F. W. Chen, *J. Mol. Graphics*, 2012, **38**, 314.
65 X. X. Wang, X. Liu, Q. Zhang and H. S. Chen, *Acta Phys. Sin.*, 2017, **66**, 103601.
66 P. B. Armentrout, *Science*, 1991, **251**, 175.
67 D. Schroder, S. Shaik and H. Schwarz, *Acc. Chem. Res.*, 2000, **33**, 139.
68 D. Kiriya, P. Lobaccaro, H. Y. Y. Nyein, P. Taheri, M. Hettick, H. Shiraki, C. M. Sutter-Fella, P. D. Zhao, W. Gao, R. Maboudian, J. W. Ager and A. Javey, *Nano Lett.*, 2016, **16**, 4047.
69 M. C. He, F. P. Kong, G. P. Yin, Z. Lv, X. D. Sun, H. Y. Shi and B. Gao, *RSC Adv.*, 2018, **8**, 14369.